Supporting Information

Source Apportionment of Urban Particulate Matter using Hourly Resolved Trace Metals, Organics, and Inorganic Aerosol Components

Cheol-Heon Jeong[1], Jon M. Wang[1], Greg J. Evans[1]

[1]Southern Ontario Centre for Atmospheric Aerosol Research, University of Toronto, Toronto, M5S 3E5, Canada

Correspondence to: Cheol-Heon Jeong (ch.jeong@utoronto.ca) and Greg J. Evans (greg.evans@utoronto.ca)

Detection limit and analytical uncertainties for Xact trace metal and Aethalometer black carbon measurements

Multiple measurements of HEPA-filtered air and external metal standards were conducted to determine the instrument detection limits (DL) and analytical uncertainties of each metal. Average plus three times of standard deviation of the background corrected filter measurements (i.e. filtered air sampling) were used as the DL for each trace metal. The relative uncertainty (w) was estimated using Eq. 1 as follows;

$$w = \frac{1}{n}\sum_{m=1}^{n}\frac{\sqrt{(C_{i,std}-C_{i,measured})^2}}{C_{i,std}} \quad (1)$$

where n is the number of replicates, $C_{i,std}$ and $C_{i,\,measured}$ are the standard and observed concentrations of the metal species i, The overall analytical uncertainty of each metal was estimated by considering the relative analytical uncertainty (w) from the metal standard measurements and the additional 5% of uncertainty from flow rates. The detection limit for Aethalometer black carbon (BC) was determined by using filtered air and quantified as the mean plus three times the standard deviation of the concentration in the filtered air measurement. The analytical uncertainty in BC measurements was set to be 30%. The detection limit, analytical uncertainty, and average concentrations of trace metals and BC are summarized in Table S1.

ACSM Organic and inorganic composition measurements

The average and standard deviation of the response factor (RF) value for nitrate and the relative ionization efficiencies (RIE) for ammonium were 2.88E-11 ± 8.19E-12 and 7.08 ± 1.26, respectively. The measured RF and RIE for sulphate during the winter campaign were 1.05E-11 ± 3.40E-12 and 0.76 ± 0.17, respectively, whereas a default RIE of 1.2 was used for the summer and spring sulphate measurement. A default RIE of 1.4 was assumed for organics over the entire campaigns.

The detection limit was estimated as described in Ng et al. (2011). Blank tests were conducted by introducing filtered air for 5 days and used to validate the stability and quantify the detection limit for each species. The 1 hr detection limits for organics (OA), sulphate, nitrate, and ammonium were 0.45 µg/m^3, 0.1 µg/m^3, 0.04 µg/m^3, and 0.4 µg/m^3, respectively. The

analytical uncertainties for sulphate and nitrate were set to 15%, while the uncertainties of 30% and 25% were used for OA and ammonium, respectively. Chloride was excluded in this study due to poor signal sensitives.

To compensate for particle losses in the ACSM, a collection efficiency (CE) must be applied. However, the CE can vary due to particle chemistry and water contents, which resulted in a high uncertainty in the assumption of CE (Canagaratna et al., 2007; Matthew et al., 2008; Middlebrook et al., 2012). The CE is also largely dependent on particle size due to the transmission efficiency of the aerodynamic focusing lens, which is limited at larger particles (> ~1 µm in vacuum aerodynamic diameter).

In this source apportionment study we assumed that the CE was 0.5 for all species. This value represented an effective CE since it also incorporated the typical ratio of 1.13 between $PM_{2.5}$ and PM_1 at this site. The typical ratio of $PM_{2.5}$ to PM_1 was empirically estimated by comparing measured size distributions of particles in the size range of 0.006 µm to 2.5 µm. Essentially, the actual CE of the ACSM for PM_1 was likely closer to 0.57 (i.e. 0.5×1.13). Scaling of the ACSM's PM_1 values up to $PM_{2.5}$ was achieved by reducing the CE down to 0.5. In order to evaluate the scaling, the ACSM data using a CE of 0.5 were compared with filter-based $PM_{2.5}$ speciation measurements. Daily $PM_{2.5}$ speciation data using filter-based samplers collected on every third day at the rooftop of the SOCAAR lab, a Canadian National Air Pollution Surveillance (NAPS, Dabek-Zlotorzynska et al., 2011) station, were available during the winter campaign period. As shown in Fig. S1, comparisons between the ACSM sulphate, nitrate, and ammonium data and the NAPS $PM_{2.5}$ filter measurements exhibited good agreement, suggesting the effectiveness of the empirical ACSM scaling and the similarity of the $PM_{2.5}$ and PM_1 composition at the urban site. In addition, the total species concentration of organics, sulphate, nitrate, and ammonium by the ACSM was compared with the $PM_{2.5}$ mass measured by a $PM_{2.5}$ monitor (SHARP 5030, Thermo Sci. Inc.). As shown in Fig. S2 (a, c), a higher correlation with a slope closer to unity was observed in the cold months as compared to the relationship in the warm months. The seasonal variations of the ratio of the total ACSM to $PM_{2.5}$ likely arose due to seasonal variability in the PM composition and hence CE. The higher CE for the winter season was consistent with findings of Middlebrook et al. (2012), who demonstrated that PM containing high ammonium nitrate can be more efficiently collected by an AMS than other inorganic and organic species. In the present study, ammonium nitrate was the dominant species in the cold months. To evaluate the effective CE applied to the ACSM data, the reconstructed mass from the ACSM and the Xact data was also calculated and compared to the $PM_{2.5}$ mass (Fig. S2b, d). Detailed calculation of the reconstructed mass is fully described elsewhere (e.g. Dabek-Zlotorzynska et al., 2011). In brief, the reconstructed mass concentrations include organics, sulphate, nitrate, ammonium, crustal matter oxides (3.48[Si]+1.63[Ca]+2.42[Fe]+1.41[K]+1.94[Ti]), trace element oxides (1.47[V]+ 1.29[Mn]+ 1.27[Ni]+ 1.25[Cu]+ 1.24[Zn]+ 1.32[As]+ 1.08[Pb]+ 1.2[Se]+ 1.37[Sr]), and particle bound water ($0.32([SO_4^{2-}]+ [NH_4^+])$). As depicted in Fig. S2 and Table S2, the reconstructed mass and the measured $PM_{2.5}$ mass concentration show good agreement with slopes near 1.0 and r^2 values of 0.74 and 0.86 in the warm and cold months, respectively.

Data preparation for the PMF analysis

Input data and uncertainty matrices for trace metals, inorganic ions, and black carbon were prepared by classifying data into three groups: data above the detection limit, data below the detection limit (BDL), and missing data. The input concentrations for BDL were replaced by half of the DL of the associated species and their corresponding errors were set at 5/6 times DL. For missing data, the median of all the concentrations measured for the given species was used as its input concentration and its error was set at 4 times the median value in order to minimize its effect on the PMF solution as described in previous PMF studies (e.g. Polissar et al., 2001). However, in order to ensure negligible influences of missing data in the PMF analysis, uncertainties for species having very low median values (i.e. trace metals) were increased. Uncertainties of missing data for Ni and V were set

at 50 times median values, while 20 times median values were used for the uncertainties of missing values for Pb, As, and Se in this study. Trace metals containing many BDL measurements (> 95%) were excluded in the analysis (i.e. Cr, Co, Rb, Ag, Cd, Sn, and Hg). Metal data measured from 00:30 to 01:00 (local time) were also excluded due to their high background levels. Elemental sulphur was also excluded since sulphate was measured by the ACSM that was used in the receptor modeling. In order to avoid the strong short-term impacts of a fireworks event, chemical speciation data on May 20, 2013 (Victoria Day) were considered as outliers and excluded from the PMF analysis.

The data and uncertainty matrices for OA mass spectra were calculated according to the method described by Ulbrich et al. (2009) and prepared by the Igor Pro based PMF evaluation tool kit (PET). A total of 121 m/z values between m/z 12 and m/z 148 were included. In addition to the uncertainties described above, a global 5% uncertainty was applied and all PMF analyses were run in the robust mode.

Additionally, variables with high noise intensities were down-weighted based on their signal-to-noise ratios (S/N) to reduce the influence of poorly resolved signals on the PMF solution. In this study, the S/N ratio was estimated by the revised S/N calculation suggested by EPA PMF 5.0 as follows:

$$\left(\frac{S}{N}\right)_j = \frac{1}{n}\sum_{i=1}^{n}\frac{x_{ij}-\sigma_{ij}}{\sigma_{ij}} \qquad if\ x_{ij} > \sigma_{ij}$$

$$\left(\frac{S}{N}\right)_j = 0 \qquad if\ x_{ij} < \sigma_{ij} \qquad (2)$$

where x_{ij} is the concentration of the j^{th} species in the i^{th} samples and σ_{ij} is the user defined analytical uncertainty. Chemical elements in the PMF analysis were classified into two groups based on their signal-to-noise ratio: good (S/N ≥ 1) and weak (S/N < 1) species. The uncertainties of weak species were increased by a factor of 3.

Hourly resolved chemical speciation data

A summary of Xact metals, ACSM organic and inorganic species, and Aethalometer BC data measured in the warm and cold months is presented in Table S1. On average, organic aerosol was the predominant component, accounting for 58% and 33% of the reconstructed PM mass in the warm months and cold months, respectively, with the highest monthly average of 11.9 μg/m^3 in July. Nitrate (33%) was the largest component in January and February, while sulphate (9%) was the second largest species in June and July. The highest concentrations of the crustal metal oxides (i.e. Si, K, Ca, Ti, Fe) and trace metal oxides were observed in April and May with the contributions of 15% and 7%, respectively.

While clear midday and evening peaks were observed for organics, nitrate peaked at around midnight under lower mixing heights and stagnant atmospheric conditions (Fig. S4). The distinct diurnal trends of organics and nitrate were consistently observed during the warm and cold months. Interpretation of diurnal trends of trace metal concentrations (Fig. S4) was possible as a result of the high time resolution of the Xact measurements. Mass concentrations of crustal elements Si, Ca, and Ti peaked during the morning rush hour with the second peak in the afternoon. Diurnal variations of supporting parameters including NOx and traffic counts are shown in Figs. S5 and S6. The diurnal trends of Ca and Ti elements were highly correlated with traffic counts with broad peaks during the daytime, suggesting that these crustal elements are resuspended into the air as a result of traffic induced turbulence during the daytime. Concentrations of Mn, Fe, and Zn that peaked during the morning rush hour were directly comparable to the diurnal variations of black carbon (r > 0.8) and NOx (r > 0.8). These trace metals can be associated with non-tailpipe emissions, i.e. tire/brake wear. No clear diurnal pattern was observed for Se, Br, and Pb, implying industrial and/or regional sources as opposed to local traffic impacts.

References

Canagaratna, M., Jayne, J., Jimenez, J. L., Allan, J. A., Alfarra, R., Zhang, Q., Onasch, T., Drewnick, F., Coe, H., Middlebrook, A., Delia, A., Williams, L., Trimborn, A., Northway, M., Kolb, C., Davidovits, P., and Worsnop, D.: Chemical and microphysical characterization of aerosols via Aerosol Mass Spectrometry, Mass Spectrom. Rev., 26, 185-222, 2007.

Dabek-Zlotorzynska, E., Dann, T. F., Martinelango, P. K., Celo, V., Brook, J. F., Mathieu, D., Ding, L., and Austin, C. C.: Canadian National Air Pollution Surveillance (NAPS) PM2.5 speciation program: Methodology and PM2.5 chemical composition for the years 2003-2008, Atmos. Environ., 45, 673-686, 2011.

Matthew, B. M., Middlebrook, A. M., and Onasch, T. B.: Collection efficiencies in an Aerodyne aerosol mass spectrometer as a function of particle phase for laboratory generated aerosols, Aerosol Sci. Tech., 42, 884-898, 2008.

Middlebrook, A. M., Bahreini, R., Jimenez, J. L., and Canagaratna, M. R.: Evaluation of composition-dependent collection efficiencies for the Aerodyne aerosol mass spectrometer using field data, Aerosol Sci. Tech., 46, 258-271, 2012.

Ng, N. L., Herndon, S. C., Trimborn, A., Canagaratna, M. R., Croteau, P. L., Onasch, T. B., Sueper, D.,Worsnop, D. R., Zhang, Q., Sun, Y. L., and Jayne, J. T.: An Aerosol Chemical Speciation Monitor (ACSM) for routine monitoring of the composition and mass concentrations of ambient aerosol, Aerosol Sci. Tech., 45, 770-784, 2011.

Polissar, A. V., Hopke, P. K., and Poirot, R. L.: Atmospheric aerosol over Vermont: Chemical composition and sources, Environ. Sci. Technol., 35, 4604-4621, 2001.

Ulbrich, I. M., Canagaratna, M. R., Zhang, Q., Worsnop, D. R., and Jimenez, J. L.: Interpretation of organic components from Positive Matrix Factorization of aerosol mass spectrometric data, Atmos. Chem. Phys., 9, 2891-2918, doi:10.5194/acp-9-2891-2009, 2009.

Table S1. Descriptive statistics, detection limit, analytical uncertainty, and the percentage of data that is missing or below the detection limit (BDL) for hourly measurements of trace metals, black carbon, and organic/inorganic PM species during the warm months (April 5-July 14, 2013) and cold months (November 25, 2013- February 11, 2014).

	Month	Mean ($\mu g/m^3$)	Median ($\mu g/m^3$)	Standard Deviation ($\mu g/m^3$)	Detection Limit ($\mu g/m^3$)	Analytical Uncertainty (%)	Missing (%)	BDL (%)
Si	Warm	1.20E-01	5.35E-02	1.17E-01	1.07E-01	15	15	74
	Cold	6.51E-02	5.35E-02	3.68E-02				
K	Warm	6.18E-02	4.70E-02	6.37E-02	1.11E-02	15	15	16
	Cold	4.84E-02	4.47E-02	2.32E-02				
Ca	Warm	1.08E-01	7.73E-02	1.22E-01	2.62E-02	16	15	32
	Cold	6.25E-02	3.80E-02	7.60E-02				
Ti	Warm	4.89E-03	4.09E-03	4.44E-03	1.88E-03	10	15	38
	Cold	2.64E-03	2.06E-03	2.47E-03				
V	Warm	2.46E-04	1.26E-04	3.00E-04	2.53E-04	11	15	82
	Cold	1.81E-04	1.26E-04	1.73E-04				
Mn	Warm	2.73E-03	2.00E-03	2.81E-03	3.72E-04	10	15	18
	Cold	2.19E-03	1.61E-03	2.56E-03				
Fe	Warm	1.14E-01	9.09E-02	1.06E-01	2.18E-02	15	15	20
	Cold	6.95E-02	5.85E-02	5.01E-02				
Ni	Warm	2.90E-04	1.67E-04	1.06E-03	3.35E-04	18	15	89
	Cold	2.20E-04	1.67E-04	5.11E-04				
Cu	Warm	4.72E-03	3.40E-03	9.04E-03	1.75E-03	10	15	42
	Cold	2.31E-03	1.79E-03	2.07E-03				
Zn	Warm	1.17E-02	7.87E-03	1.31E-02	1.36E-03	10	15	16
	Cold	1.49E-02	9.51E-03	2.03E-02				
As	Warm	2.89E-04	1.50E-04	4.72E-04	3.00E-04	10	15	88
	Cold	2.08E-04	1.50E-04	2.51E-04				
Se	Warm	4.40E-04	1.99E-04	6.51E-04	1.99E-04	10	15	57
	Cold	5.66E-04	2.19E-04	9.86E-04				
Br	Warm	3.27E-03	2.78E-03	2.71E-03	1.96E-04	11	15	17
	Cold	4.38E-03	3.33E-03	3.87E-03				
Sr	Warm	6.44E-04	4.26E-04	9.03E-04	8.52E-04	10	15	90
	Cold	4.99E-04	4.26E-04	2.96E-04				
Ba	Warm	3.55E-03	2.45E-03	4.36E-03	1.56E-03	15	15	57
	Cold	1.52E-03	7.81E-04	1.45E-03				
Pb	Warm	2.89E-03	2.44E-03	2.35E-03	4.31E-04	10	15	19
	Cold	3.41E-03	2.16E-03	1.16E-02				
BC	Warm	7.84E-01	6.05E-01	6.30E-01	5.27E-02	30	3	3
	Cold	5.67E-01	4.67E-01	3.65E-01				
Organics	Warm	5.53E+00	3.97E+00	5.55E+00	4.50E-01	30	5	6
	Cold	3.60E+00	2.87E+00	2.47E+00				
Sulphate	Warm	7.95E-01	4.45E-01	9.02E-01	1.00E-01	15	5	8
	Cold	1.38E+00	1.16E+00	9.25E-01				
Nitrate	Warm	7.26E-01	4.19E-01	9.27E-01	4.00E-02	15	5	6
	Cold	3.41E+00	2.03E+00	3.64E+00				
Ammonium	Warm	7.07E-01	4.89E-01	6.78E-01	4.00E-01	25	5	36
	Cold	1.28E+00	9.20E-01	1.12E+00				

Data below the detection limit were replaced by one-half of the detection limit values.

Table S2. The ratios of reconstructed elements to the measured $PM_{2.5}$ mass during the warm months (April 5-July 14, 2013) and cold months (November 25, 2013- February 11, 2014).

	Organics	Sulphate	Nitrate	Ammonium	CMO[a]	TEO[a]	PBW[a]	Reconstructed Total Mass
Warm Months	0.643	0.093	0.086	0.084	0.120	0.004	0.057	1.087
Cold Months	0.356	0.133	0.342	0.127	0.051	0.003	0.083	1.095

[a] CMO: crustal matter oxides, TEO: trace element oxides, PBW: particle bound water

Table S3. A summary (mean ± standard deviation) of meteorological conditions and gaseous measurements.

	Temp (°C)	RH (%)	WS (m/s)	SO_2 (ppb)	NOx (ppb)	CO (ppb)	UFP[a] (#/cm^3)	Traffic count (veh #/hr)
April, 2013	8±5	63±15	2.1±1.0	<0.1	20±12	306±81	17200± 8300	n/a
May, 2013	16±5	53±20	1.8±0.9	<0.1	18±11	336±99	17400± 12200	n/a
June, 2013	19±4	63±17	1.6±0.8	<0.1	16±10	355±98	14800± 9300	n/a
July, 2013	23±3	69±15	1.3±0.8	<0.1	12±6	406±79	13200± 9200	n/a
Average	16±7	61±18	1.8±0.9	<0.1	17±11	344±97	16000± 10200	n/a
Dec., 2013	-2±5	68±12	2.3±1.1	0.7±0.9	29±17	261±95	16800± 8800	740±410
Jan., 2014	-7±7	65±12	3.5±1.7	1.2±1.4	25±18	264±81	18700± 8900	870±440
Feb., 2014	-7±4	68±10	2.4±1.1	1.0±0.9	n/a	335±105	20100± 10500	760±400
Average	-5±6	66±12	2.8±1.5	0.9±1.1	28±17	268±96	18000± 9200	810±430

[a]number concentration of ultrafine particles (UFP) in the size range 8-560 nm.

Table S4. Correlation (Spearman r) of PMF_{metal} resolved factors with supporting variables for both warm and cold month periods. The highest correlation coefficients for each case are denoted in bold.

Factor	UFP	NO_X	CO	SO_2[a]	Temp	RH	Traffic[a]
Ca-Si	0.24	0.16	0.28	-0.10	**0.31**	**-0.38**	-0.25
Cu-Ba	0.19	0.26	**0.57**	-0.33	**0.38**	-0.14	**-0.47**
Zn-rich	0.27	**0.39**	0.24	**0.43**	-0.06	0.15	-0.02
Mn-rich	**0.39**	0.38	**0.40**	0.21	0.16	-0.11	-0.15
K-rich	0.07	0.12	**0.46**	0.02	0.32	0.10	-0.27
Pb-rich	0.12	0.18	**0.28**	0.24	0.16	0.17	-0.17
V-Ni	0.23	0.05	0.14	**0.41**	-0.03	-0.06	0.06
Se-rich	-0.02	-0.01	0.21	0.15	0.17	**0.32**	0.01

[a] Correlation analysis for the cold months only

Table S5. Correlation (Spearman r) of PMF_{org} resolved factors with supporting variables. The highest correlation coefficients for each case are denoted in bold.

Factor	UFP	NO_X	CO	SO_2[a]	Temp	RH	Traffic[a]
HOA	**0.42**	**0.39**	**0.63**	0.04	0.29	0.00	-0.29
COA	0.29	0.17	**0.37**	0.11	0.12	0.15	-0.04
BBOA	0.19	0.25	**0.36**	**0.33**	0.00	**0.27**	-0.09
OOA	0.04	-0.15	**0.62**	-0.29	**0.61**	0.16	-0.46
LV-OOA	0.01	-0.08	**0.42**	0.13	0.35	0.23	-0.19

[a] Correlation analysis for the cold months only

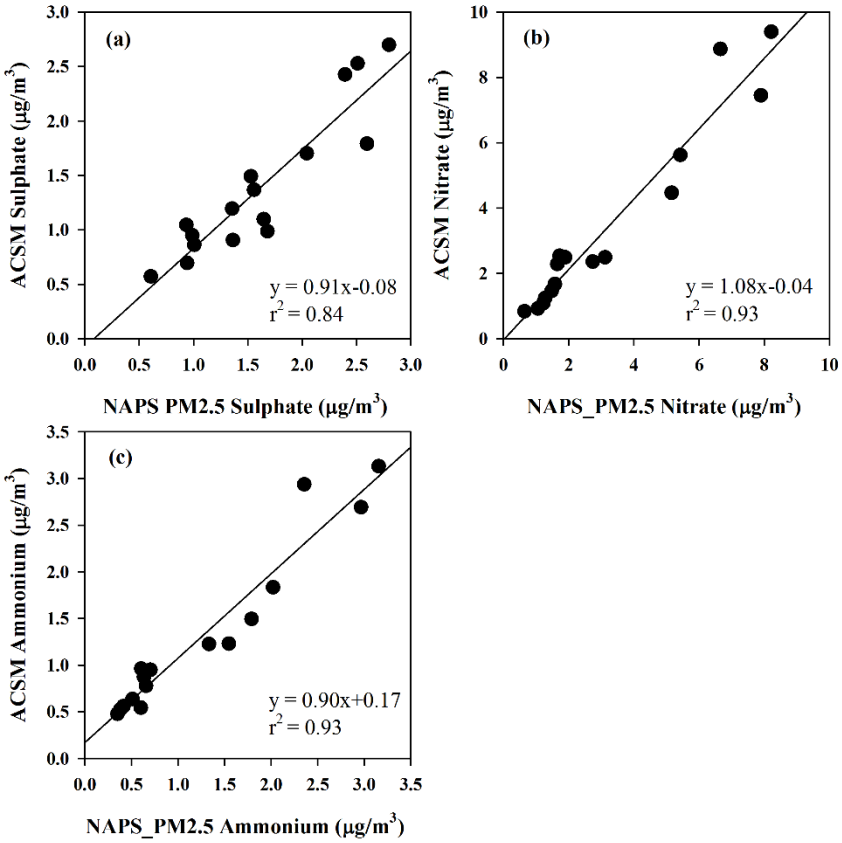

Figure S1. Comparison of daily averaged ACSM sulphate (a), nitrate (b), and ammonium (c) with NAPS filter-based $PM_{2.5}$ speciation measurements from November 25, 2013 to February 11, 2014 (n=16).

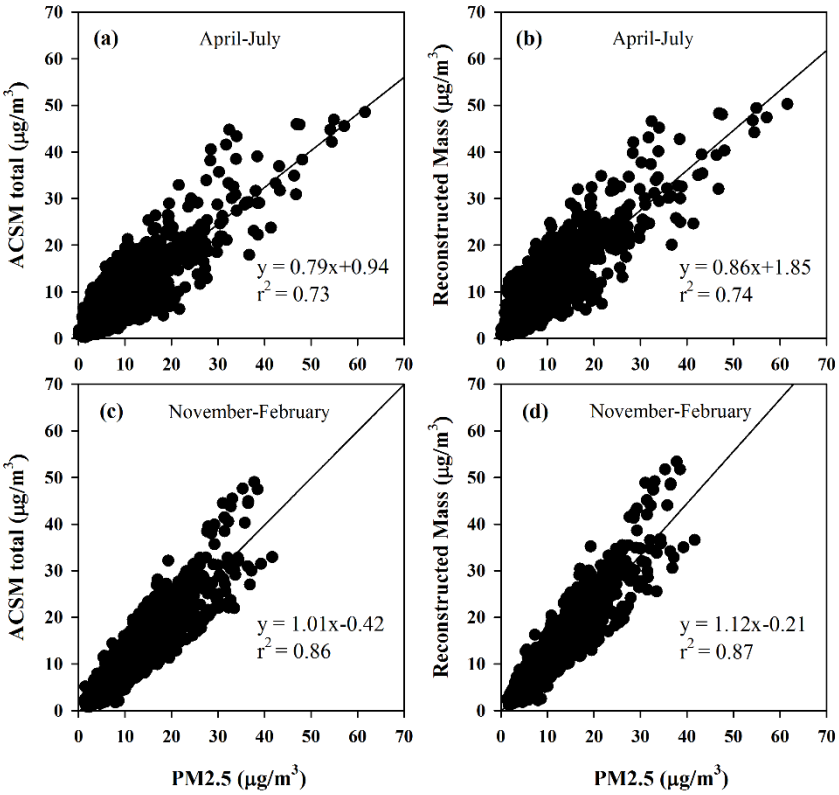

Figure S2. Comparison of hourly averaged ACSM total mass (sulphate+nitrate+ammonium+organics, a and c) and the reconstructed PM mass concentrations (b and d) with the measured $PM_{2.5}$ concentrations in the warm months (a and b) and cold months (c and d).

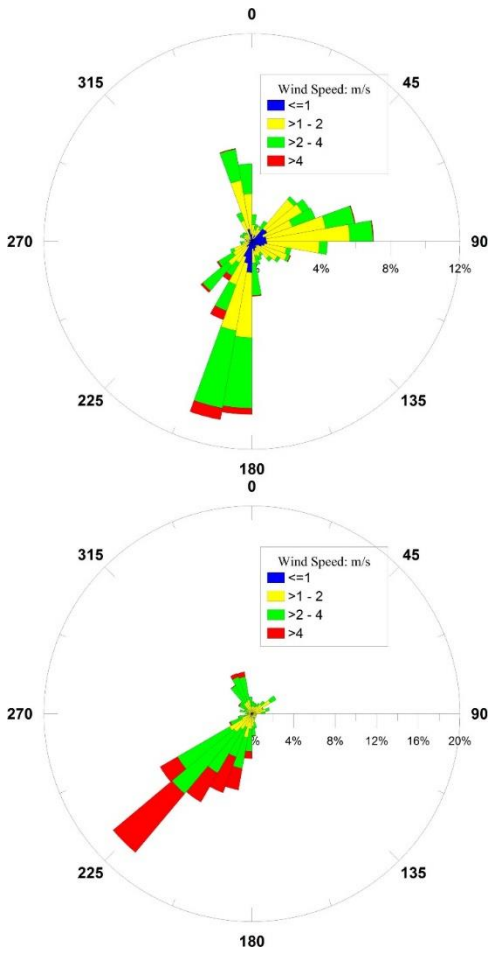

Figure S3. Windrose plots for the warm (a) and cold (b) month campaign periods in Toronto.

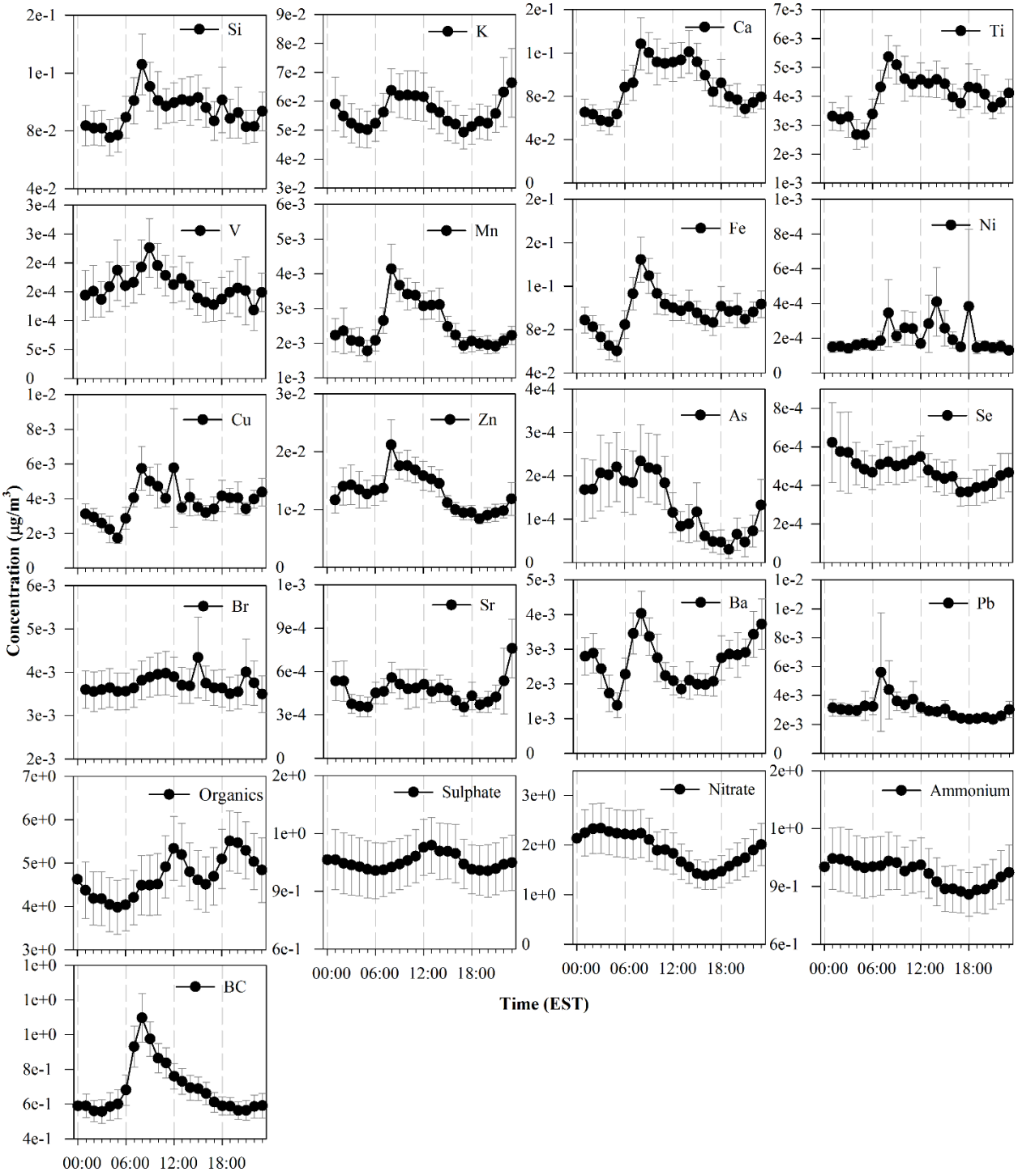

Figure S4. Diurnal variations of chemical species measured by the ACSM, Xact, and Aethalometer during the entire measurement period. Error bars represent the 95% confidence intervals.

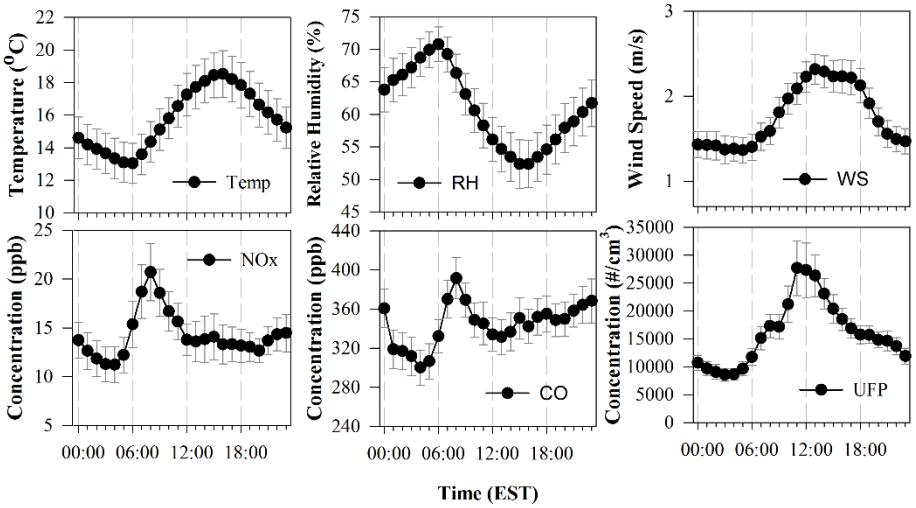

Figure S5. Diurnal variations of meteorological parameters and gaseous pollutants measured from April 5 to July 14, 2013. Error bars represent the 95% confidence intervals.

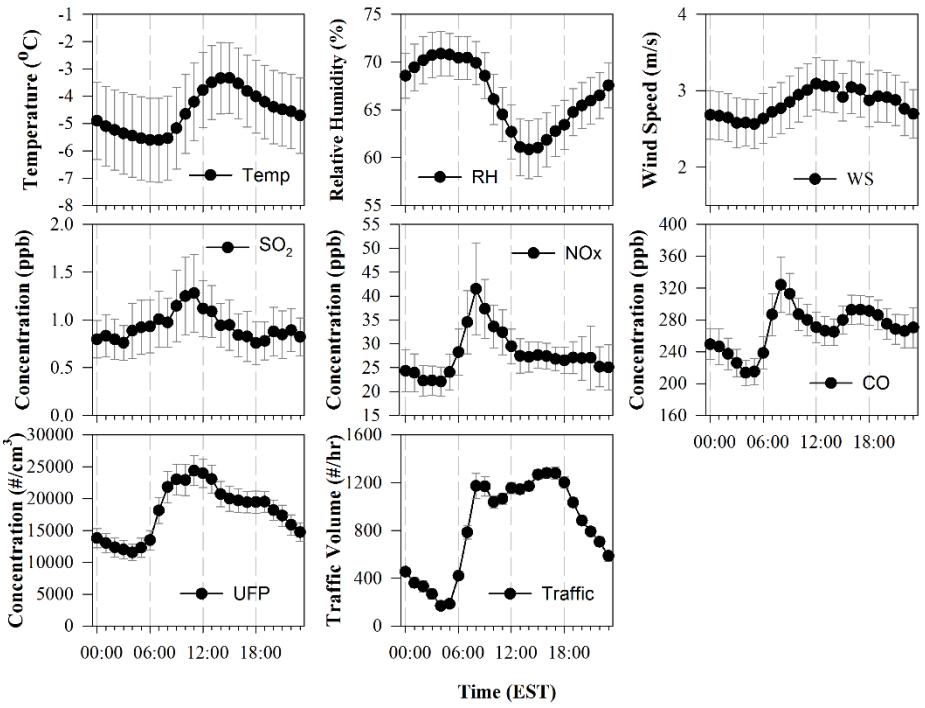

Figure S6. Diurnal variations of meteorological parameters, gaseous pollutants, and traffic density measured from November 25, 2013 to February 11, 2014. Error bars represent the 95% confidence intervals.

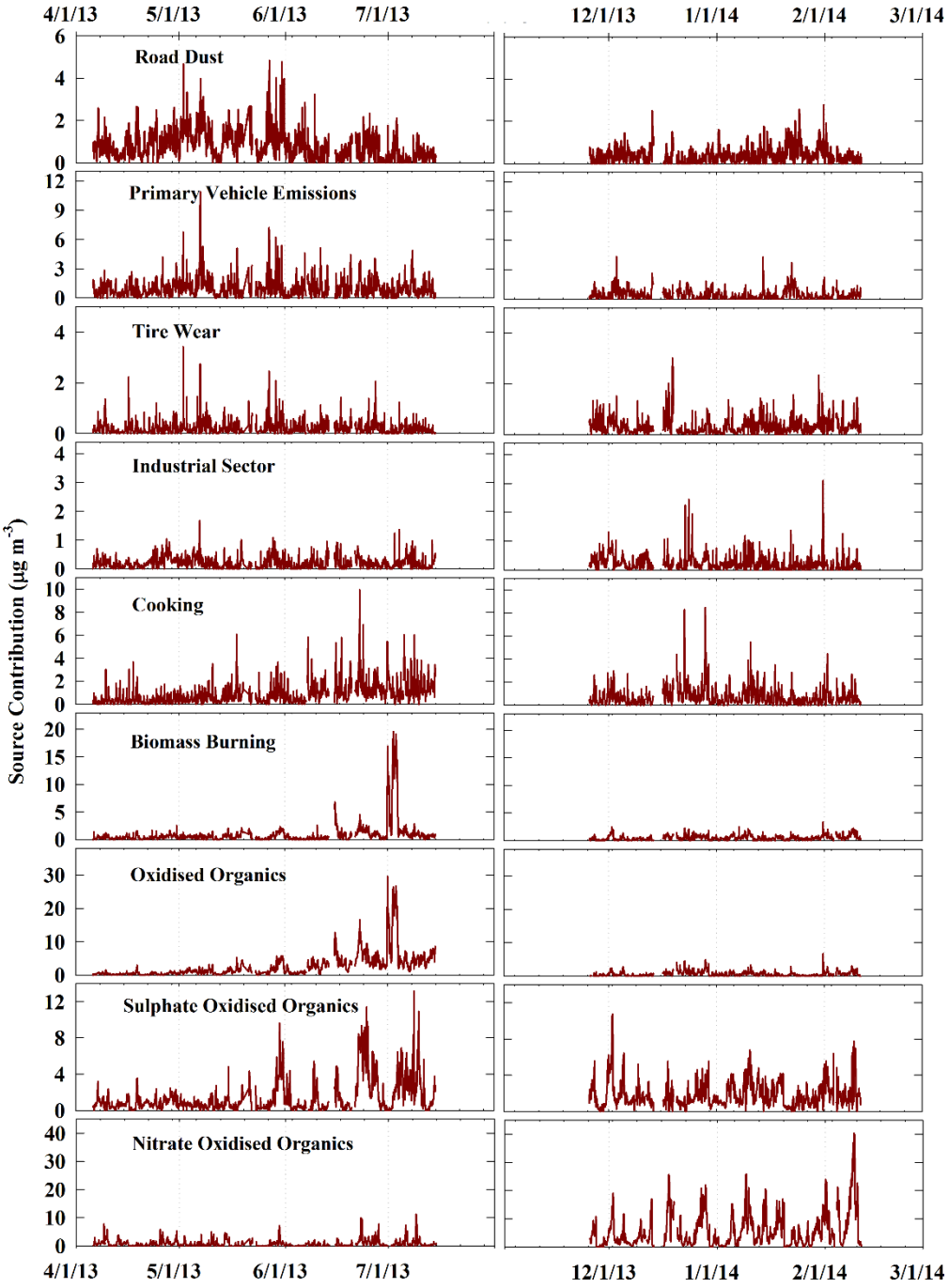

Figure S7. Source contributions of 9 factors: Road Dust, Primary Vehicle Emissions, Tire Wear, Industrial Sector, Cooking, Biomass Burning, Oxidised Organics, Sulphate and Oxidised Organics, and Nitrate and Oxidised Organics from the PMF_{Full} analysis. Left and right figures represent warm months and cold months, respectively.

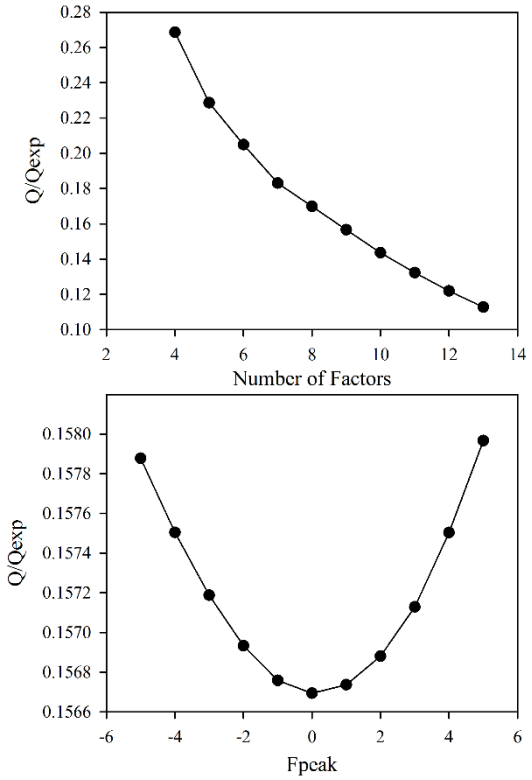

Figure S8. Change of Q/Q_{exp} as a function of Fpeak rotations for the 9-factor solution of the PMF_{Full} analysis.

Figure S9. Conditional probability function (CPF) plots for the 9 factors: (a) Road Dust, (b) Primary Vehicle Emissions, (c) Tire Wear, (d) Industrial Sector, (e) Cooking, (f) Biomass Burning, (g) Oxidised Organics, (h) Sulphate and Oxidised Organics, (i) Nitrate and Oxidised Organics from the PMF_{Full} analysis. The CPF threshold was set to the top 25th percentile.

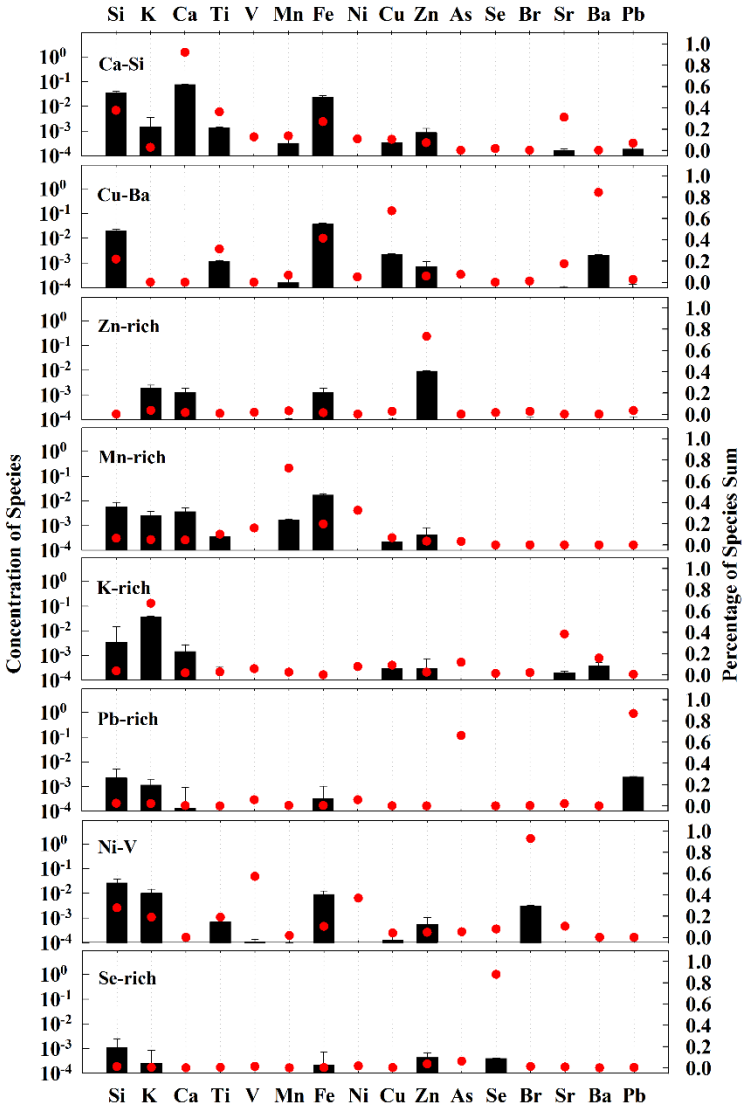

Figure S10. Source profiles of the 8 factor solution from the PMF_{metal} analysis. Black bars on the left y-axis represent the concentration of each species apportioned to the factor. Error bars represent uncertainties estimated by 100 bootstrap runs. Red dots on the right y-axis represent the percentage of each species apportioned to the factor.

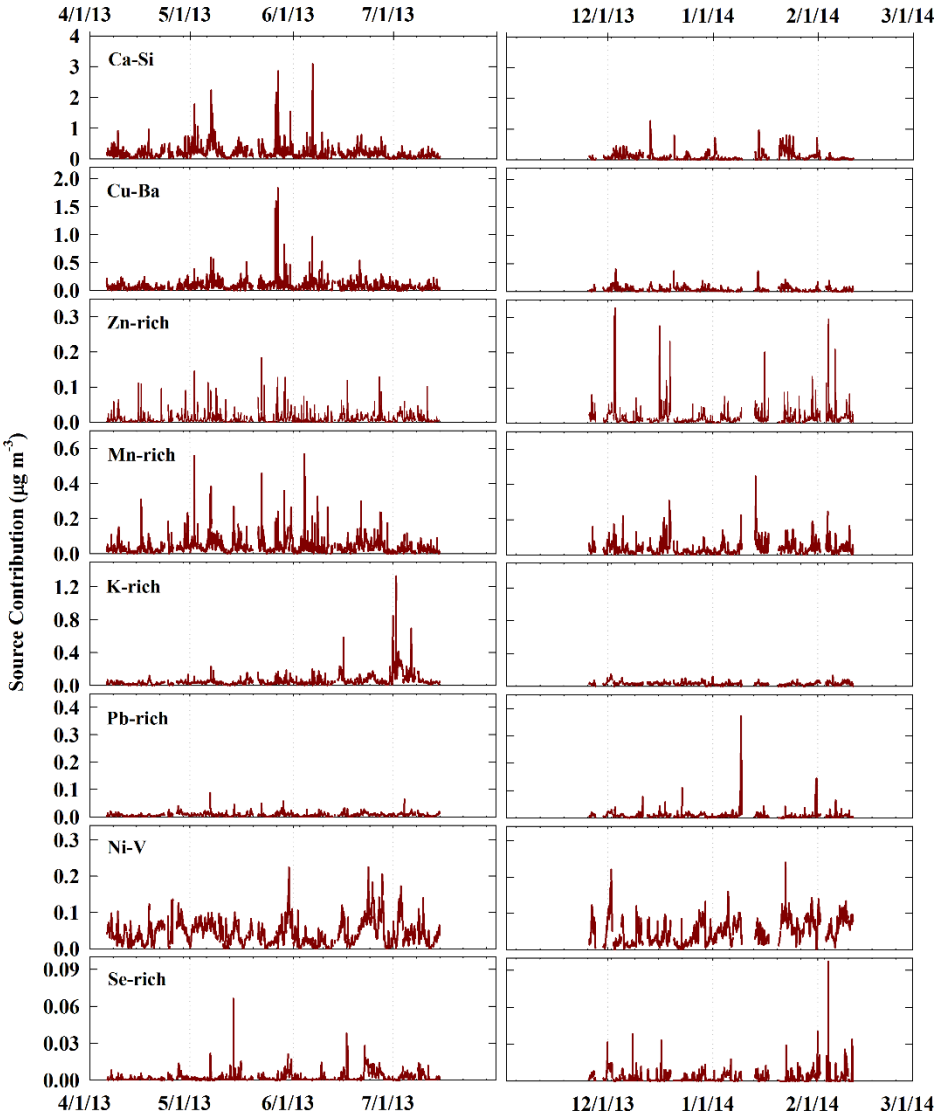

Figure S11. Source contributions of the 8 factor solution from the PMF_{metal} analysis. Left and right figures represent warm months and cold months, respectively.

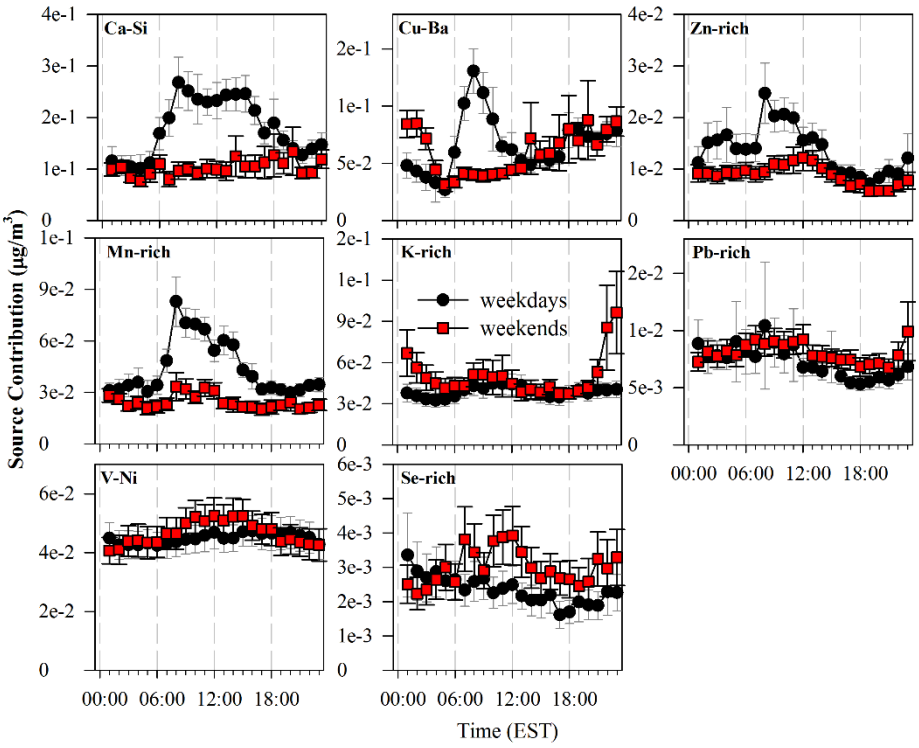

Figure S12. Diurnal trends for the traffic-related (Ca-Si, Cu-Ba, Zn-rich, and Mn-rich), biomass burning (K-rich), industry (Pb-rich), oil-combustion (V-Ni), and coal combustion (Se-rich) factors from the PMF_{metal} analysis. The traffic-related factors demonstrated a strong diurnal trend consistent with traffic pattern during the morning rush hours.

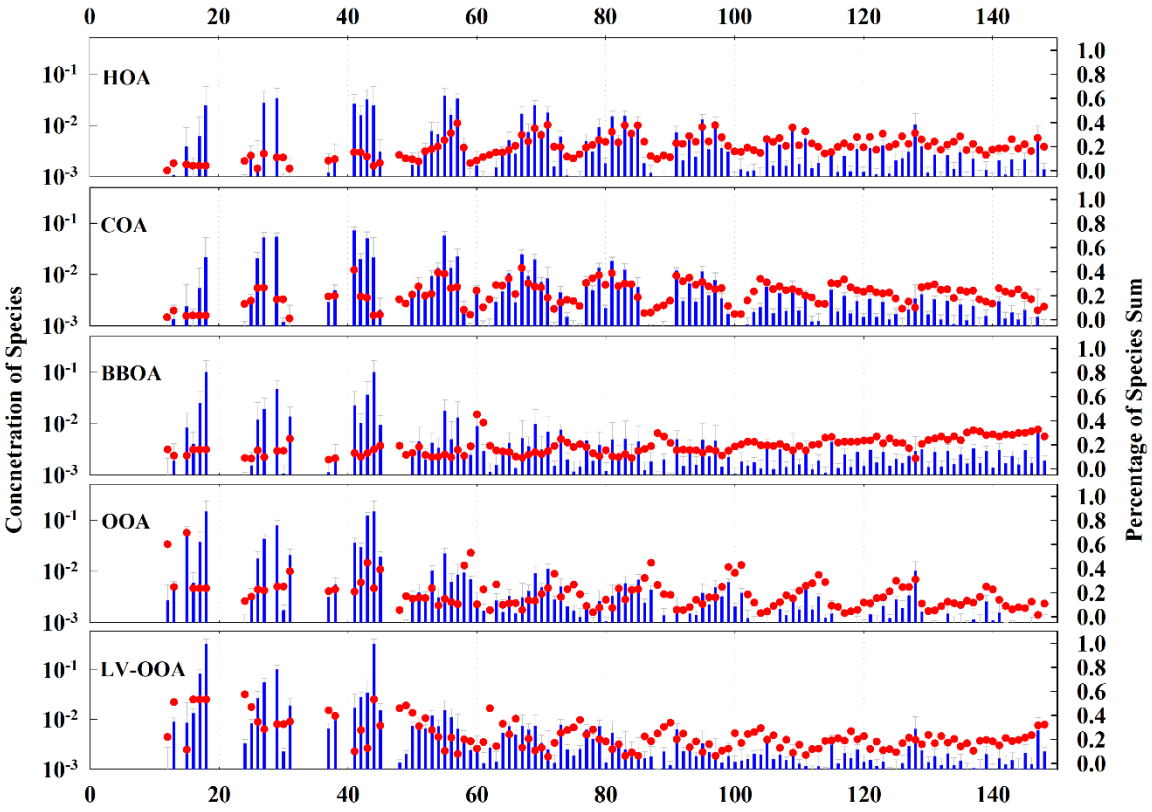

Figure S13. Source profiles of PMF_{org} resolved organic factors: HOA, COA, BBOA, OOA, and LV-OOA. The fraction of species sum on the right y-axis for each factor represents the percentage of each species apportioned to the factor. Blue bars on the left y-axis represent the concentration of each species apportioned to the factor. Error bars represent uncertainties estimated by 100 bootstrap runs. Red dots on the right y-axis represent the percentage of each species apportioned to the factor.

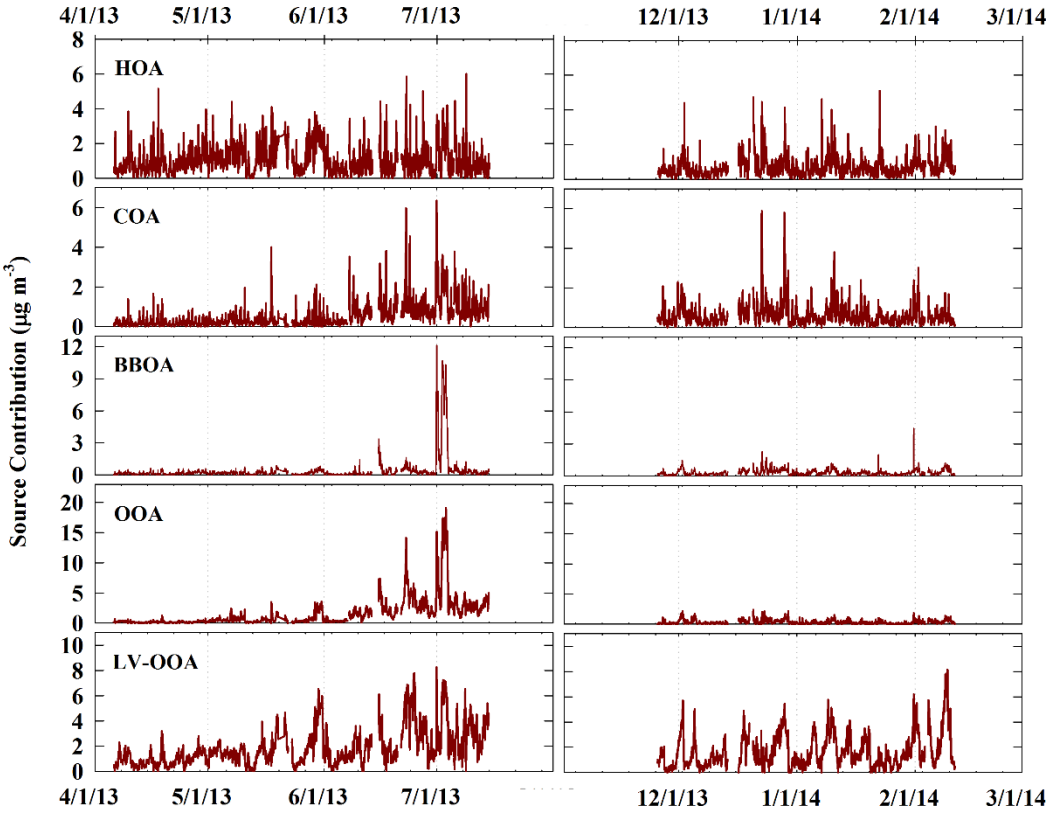

Figure S14. Source contributions of PMF_{org}-resolved organic factors: HOA, COA, BBOA, OOA, and LV-OOA. Left and right figures represent warm months and cold months, respectively.

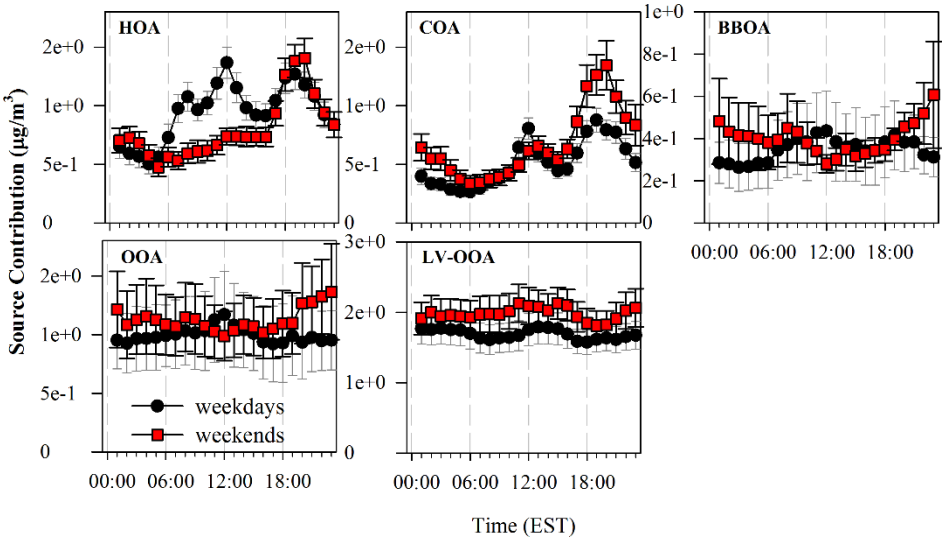

Figure S15. Diurnal trends of PMF_{org}-resolved organic factors: HOA, COA, BBOA, OOA, and LV-OOA.